Computational assessment of possible origins of the back-hopping effect in magnetic tunnel junctions

Peter Flauger, Claas Abert, and Dieter Suess
Faculty of Physics, University of Vienna, Vienna 1090, Austria
and University of Vienna Research Platform MMM Mathematics-Magnetism-Materials, University of Vienna, Vienna 1090, Austria

(Received 1 January 2023; revised 12 April 2023; accepted 12 April 2023; published 26 July 2023)

In this work we employ macrospin simulations of the magnetization dynamics obtained from the Landau-Lifshitz-Gilbert equation coupled to angular momentum transport yielded by the nonequilibrium Green's function formalism to investigate two possible origins of the back-hopping effect in magnetic tunnel junctions with one layer of a synthetic antiferromagnet as reference layer. One possible origin discussed in this work is an additional sign reversal of the dampinglike (parallel) torque component as a function of the applied voltage. The other is the destabilization and switching of the reference layer by the spin-transfer torque. We find that this destabilization gives rise to a dynamic behavior manifesting in a back-and-forth switching of the free layer, while the sign reversal of the dampinglike torque results in a second hysteresis loop.

DOI: 10.1103/PhysRevB.108.014430

I. INTRODUCTION

A magnetic tunnel junction (MTJ) usually consists of two ferromagnetic (FM) layers connected by an insulator. One of the ferromagnetic layers (the reference layer, RL) has its magnetization pinned in one direction, which can be achieved, e.g., by a large uniaxial anisotropy, or by coupling it to an antiferromagnet or hard magnetic layer via the interlayer exchange coupling. The latter has a variety of advantages [1], including the possibility to compensate the stray field of the stack by setting up a synthetic antiferromagnet, to only name one. The magnetization direction of the second layer (the free layer, FL) usually can be changed by internal or external means.

The tunnel magnetoresistance (TMR) effect of MTJs [2,3] opens up a vast variety of technological applications. One of these is the spin-transfer torque (STT) driven magnetoresistive random access memory (STT-MRAM) [4,5], which makes use of the ability to influence the magnetization direction of a ferromagnetic layer by injecting a spin-polarized current [6–9]. The basic idea is to use a writing current in order to align the free-layer magnetization either parallel or antiparallel to the reference-layer magnetization, depending on the polarity of the applied voltage. Due to the TMR effect, the parallel (antiparallel) state corresponds to a low (high) resistance, that can be determined by a smaller reading current.

One might expect that higher voltages lead to faster switching with fewer writing errors, but for some SST-MRAM cells, this is not the case. Instead, the device switches to either the low- or high-resistance state indiscriminately [10]. This means that when the voltage is gradually increased, the cell will first switch as desired but then, for larger voltages, switch back to the original state and from there on, back and forth between the two states. This so-called back-hopping effect was observed for one (e.g., in Ref. [11]) and both voltage polarities (e.g., in Ref. [10]), and it poses an obstacle for reliable STT-MRAM.

Different potential origins for this effect have been discussed, including the reduction of the anisotropy of the involved magnetic materials [12] or the quadratic nature of the dampinglike torque component in MTJs as, e.g., indicated theoretically and experimentally in Refs. [13–15]. Another possible origin is the destabilization of the reference layer by the STT, as argued in Refs. [16,17], which used a macrospin model, including a Slonczewski torque term that scales linearly with the current. In fact, this effect would be the result of basic STT properties and can therefore be expected to appear not only in MTJs, but also in STT-driven giant magnetoresistance devices, as argued by Abert *et al.* in Ref. [18]. Devolder *et al.* attempted to determine the origin of the effect by conducting time-resolved measurements of the switching in Ref. [19]. They found that for the parallel to antiparallel switching direction (P $\rightarrow$ AP) the device would first switch to AP as intended but then transition into a low-resistance state P′ that differs slightly from the original state. They also found that this state usually relaxes into the AP state when the voltage is cut off.

In this work we are going to show how both the additional sign reversal of the dampinglike torque component and the dynamic effect of the STT acting back on the reference layer would yield undesired switching behavior in stacks with a synthetic antiferromagnet as reference system. In contrast to the computational works carried out in [16–18], we are not going to assume a linear dependence of the torque on the current but instead obtain both the fieldlike and dampinglike torque from a free-electron model in a coherent transport regime.

Published by the American Physical Society under the terms of the Creative Commons Attribution 4.0 International license. Further distribution of this work must maintain attribution to the author(s) and the published article's title, journal citation, and DOI.

II. METHODS

A. Simulation of the magnetization dynamics

The underlying assumption of the concurrent simulation of the magnetization dynamics and the spin accumulation is that the local magnetization of a ferromagnetic material is due to localized electrons, while the (spin) current flowing through the stack results from the movement of the delocalized conduction electrons. However, the systems do not behave independently but mutually influence each other. In this modeling the localized electrons induce an exchange splitting to the potential felt by the conduction electrons, resulting in an spin-dependent wave function. The spin accumulation $\boldsymbol{s}$ is the local expectation value of the individual spin components and can be obtained from numerical solutions of the Schrödinger equation or, equivalently, the nonequilibrium Green's function formalism [20–23].

When the magnetization dynamics are obtained from the modified Landau-Lifshitz-Gilbert equation (LLG),

$$\frac{\partial \boldsymbol{m}}{\partial t} = -\gamma \boldsymbol{m} \times \boldsymbol{H}^{\text{eff}} + \alpha \boldsymbol{m} \times \frac{\partial \boldsymbol{m}}{\partial t} + \boldsymbol{T}, \tag{1}$$

the effect of spin accumulation on the local magnetization is accounted for by the torque:

$$\boldsymbol{T} = -\frac{J_{sd}}{\hbar M_s} \boldsymbol{m} \times \boldsymbol{s}. \tag{2}$$

Here $\boldsymbol{m}$ is the normalized local magnetization, M_s the saturation magnetization such that the local magnetization is $\boldsymbol{M} = M_s \boldsymbol{m}$, γ is the reduced gyromagnetic ratio, $\alpha = 0.05$ (if not stated otherwise) denotes the Gilbert damping parameter, and $\boldsymbol{H}^{\text{eff}}$ is the effective field. The coupling between the local magnetization and the spin accumulation is measured by the spin-split potential J_{sd}.

Assuming that the spin accumulation relaxes much faster than the local magnetization yields an iterative scheme for coupled simulations that sees the spin accumulation being updated on the basis of the current magnetization before every time step of the LLG equation [21,22].

Since the $\boldsymbol{m}$ is a unit vector, the torque $\boldsymbol{T}$ can be split into a dampinglike and a fieldlike part:

$$\boldsymbol{T} = \boldsymbol{T}_{\text{dl}} + \boldsymbol{T}_{\text{fl}}, \tag{3}$$

$$\boldsymbol{T}_{\text{fl}} = \tau_{\text{fl}} \boldsymbol{m} \times \boldsymbol{p}, \tag{4}$$

$$\boldsymbol{T}_{\text{dl}} = \tau_{\text{dl}} \boldsymbol{m} \times (\boldsymbol{m} \times \boldsymbol{p}). \tag{5}$$

In a spin-valve structure with a reference and free layer, the polarization vector $\boldsymbol{p}$ is the magnetization direction of the layer across the barrier:

$$\boldsymbol{p} = \begin{cases} \boldsymbol{m}_{\text{RL}} & \text{for torque acting on } \boldsymbol{m}_{\text{FL}} \\ \boldsymbol{m}_{\text{FL}} & \text{for torque acting on } \boldsymbol{m}_{\text{RL}} \end{cases}. \tag{6}$$

It should be apparent from (2) that the component of $\boldsymbol{s}$ parallel to $\boldsymbol{m}$ cannot change the dynamics obtained from (1). Thus the effective spin accumulation

$$\boldsymbol{s}^{\text{eff}} = -s_{\text{fl}} \boldsymbol{m} \times (\boldsymbol{m} \times \boldsymbol{p}) + s_{\text{dl}} \boldsymbol{m} \times \boldsymbol{p} \tag{7}$$

with

$$s_{\text{fl}} = \frac{\boldsymbol{s} \cdot \boldsymbol{b}_{\text{fl}}}{\boldsymbol{b}_{\text{fl}} \cdot \boldsymbol{b}_{\text{fl}}}, \tag{8}$$

$$s_{\text{dl}} = \frac{\boldsymbol{s} \cdot \boldsymbol{b}_{\text{dl}}}{\boldsymbol{b}_{\text{dl}} \cdot \boldsymbol{b}_{\text{dl}}}, \tag{9}$$

$$\boldsymbol{b}_{\text{fl}} = -\boldsymbol{m} \times (\boldsymbol{m} \times \boldsymbol{p}), \tag{10}$$

$$\boldsymbol{b}_{\text{dl}} = \boldsymbol{m} \times \boldsymbol{p} \tag{11}$$

results in the same magnetization dynamics as the original spin accumulation. Inserting (7) into (2) relates the torque coefficients with the coefficients of the effective spin accumulation:

$$\tau_{\text{fl}} = -\frac{J_{\text{sd}}}{\hbar M_s} s_{\text{fl}}, \tag{12}$$

$$\tau_{\text{dl}} = -\frac{J_{\text{sd}}}{\hbar M_s} s_{\text{dl}}. \tag{13}$$

The advantage of this might not be clear right away, but in MTJs the coefficients s_{fl} and s_{dl} obtained from the fully coherent free-electron model do not depend on the relative orientation of $\boldsymbol{m}_{\text{RL}}$ and $\boldsymbol{m}_{\text{FL}}$, as long as the bias voltage V_b is fixed [24,25]. Instead, they are constant with respect to the angle between the two magnetization directions. Consequently, it is not necessary to compute the spin accumulation in every time step of the LLG integration, as long as the voltage does not change.

The macrospin simulations presented in this work were achieved with scipy.integrate.ode using an implicit solver based on the explicit form of the LLG:

$$\begin{aligned}\frac{\partial \boldsymbol{m}(V_b)}{\partial t} = &- \frac{\gamma}{1+\alpha^2} \boldsymbol{m} \times \left\{ \boldsymbol{H}^{\text{eff}} + \frac{1}{\gamma} [\alpha \tau_{\text{dl}}(V_b) - \tau_{\text{fl}}(V_b)] \boldsymbol{p} \right\} \\ &- \frac{\alpha\gamma}{1+\alpha^2} \boldsymbol{m} \times \left[\boldsymbol{m} \times \left\{ \boldsymbol{H}^{\text{eff}} - \frac{1}{\gamma} \left[\frac{1}{\alpha} \tau_{\text{dl}}(V_b) \right.\right.\right. \\ &\left.\left.\left. + \tau_{\text{fl}}(V_b) \right] \boldsymbol{p} \right\} \right]. \end{aligned} \tag{14}$$

We will investigate the switching dynamics of two MTJ stacks with an out-of-plane uniaxial anisotropy. Both stacks are of the same general structure. The reference system is a synthetic antiferromagnet that consists of two coupled magnetic layers, the hard layer and the reference layer, separated by a nonmagnetic (NM) spacer layer. The layers are stacked along the z direction, and the reference layer is followed up first by an insulating layer and then the free layer.

To model the stacks, the effective field $\boldsymbol{H}^{\text{eff}} = \boldsymbol{H}^{\text{aniso}} + \boldsymbol{H}^{\text{IEX}}$ in Eq. (1) contains contributions from the uniaxial anisotropy and the interlayer exchange coupling in the form of a bias field acting on the reference layer. This bias field accounts for the coupling of the reference system to the hard layer as part of an antiferromagnetic reference system, without modeling the hard layer explicitly. Thus the field associated with the interlayer exchange coupling constant A_{IEX} is always directed along $\hat{z}$:

$$\boldsymbol{H}^{\text{IEX}} = \frac{A_{\text{IEX}}}{J_s L_{\text{RL}}} \hat{z}. \tag{15}$$

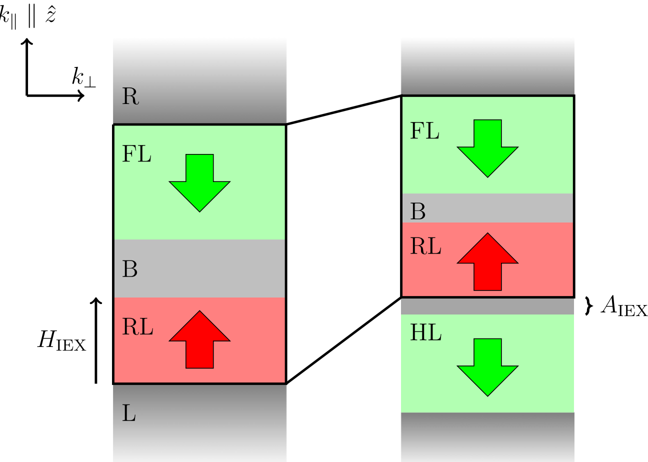

FIG. 1. The simulations account for the reference layer (RL) being antiferromagnetically coupled to a static hard layer (HL) only by introducing a bias exchange field within the reference layer. In neither the transport calculations nor the magnetization dynamics calculations, the hard layer is modeled explicitly. The barrier region is labeled as B, the nonmagnetic leads are labeled as left (L) and right (R) to be consistent with the literature [20].

Here $L_{\rm RL}$ is the thickness of the reference layer. This reduction of the scope of the simulation is shown in Fig. 1.

The uniaxial anisotropy in the magnetic layers is oriented along the out-of-plane axis, i.e., the z axis:

$$\boldsymbol{H}^{\rm aniso} = \frac{2K_u}{J_s}(\boldsymbol{m}\cdot\hat{z})\hat{z}. \tag{16}$$

Since the stray field is not included in the simulations explicitly, the values stated in Table I resemble an effective anisotropy. The value for the free-layer anisotropy correspond to critical switching fields of $\mu_0 H_c \approx 20$ mT and 17 mT for stacks A and B, respectively. Experimental studies that went into consideration for this work report values from $\approx$10 mT [15,26] to about 2.3 mT [6].

The two stacks differ only in the choice of the parameter values used for the magnetization dynamics calculations and the free-electron model. These parameters are stated in Tables I and II, respectively. Theoretical studies of the free-electron model in MTJs showed that the behavior of the torque components as a function of the bias voltage depends strongly on the parameters used [13,24], and as we will see, they can be chosen so that qualitative differences in the behavior of the dampinglike torque component for stacks A and B lead to two distinct mechanisms of writing errors.

TABLE I. Parameters of the stacks used for the time integration of Eq. (1). $A_{\rm IEX}$ is the interlayer exchange coupling constant of the synthetic antiferromagnet, $J_s = \mu_0 M_s$ is the saturation polarization, and K_u the uniaxial anisotropy.

ID	$A_{\rm IEX}$ (J/m^2)	$J_{s,\rm RL}$ (T)	$J_{s,\rm FL}$ (T)	$K_{u,\rm RL}$ (J/m^3)	$K_{u,\rm FL}$ (J/m^3)
A	4×10^{-4}	1.3	1	1.2×10^{4}	8×10^{3}
B	4×10^{-4}	1.2	1.2	1.6×10^{4}	8×10^{3}

In Ref. [21], Datta *et al.* presented a set of parameters for a three-domain model with semi-infinite ferromagnetic leads that yield a TMR behavior similar to experimental findings for MgO- and Al_2O_3-based MTJs with Fe leads. In doing so, Datta *et al.* treated the effective mass and barrier height as system parameters that also account for impurities and interface effects rather than as true material parameters. The values that characterize the two stacks A and B in this work (Table II) were chosen to lie in the general vicinity to the values stated in Ref. [21] but differ enough to result in an additional change of the dampinglike torque for stack B which is not present in stack A for $V_b \leqslant 1$ V.

B. Calculation of the spin accumulation

The spin accumulation is obtained from a fully coherent free-electron model with open-boundary conditions. This approach is justified mainly by the similarity of Δ_1 bands in bcc Fe and Co to the free-electron dispersion [24,27]. The calculations can be performed on the basis of a single-particle Hamiltonian that accounts for five domains, indexed by a variable m taking the values L (the semi-infinite nonmagnetic left lead), RL (the reference layer), B (the insulating barrier region), FL (the free layer), and R (the semi-infinite nonmagnetic right lead). Alternatively, the effects of the NM/FM interfaces can be excluded by accounting for only three domains in the model Hamiltonian: the reference layer, the barrier region, and the free layer with the two ferromagnetic layers assumed to be semi-infinite in the context of the coherent transport calculations. The discrete form of the Hamiltonian with spatially varying effective mass m^* [28],

$$\hat{H}(z) = -\frac{\hbar^2}{2m^*(z)}\left[\frac{\partial^2}{\partial x^2}+\frac{\partial^2}{\partial y^2}\right] - \frac{\hbar^2}{2}\frac{\partial}{\partial z}\left(\frac{1}{m^*(z)}\frac{\partial}{\partial z}\right) + \hat{U}(z), \tag{17}$$

on a one-dimensional finite-difference mesh with N sample points indexed by i or j and discretization length a is given by

$$H_{ij}(k_\perp) = \begin{cases} h_m(k_\perp) + v_i I_2 & i = j \\ -t_m I_2 & j = i \pm 1 \\ 0_{2,2} & \text{else} \end{cases} \tag{18}$$

for points lying within the domain m, and by

$$H_{ij}(k_\perp) = \begin{cases} [h_m(k_\perp) + h_n(k_\perp)]/2 + v_i I_2 & i = j \\ -t_m I_2 & j = i-1 \\ -t_n I_2 & j = i+1 \\ 0_{2,2} & \text{else} \end{cases} \tag{19}$$

on the interfaces between the domains m and n [21]. Note that all entries are 2×2 matrices. I_2 denotes the 2×2 identity matrix, $0_{2,2}$ is a zero matrix of the same size, and

$$t_m = \frac{\hbar^2}{2m_m^* a^2} \tag{20}$$

TABLE II. Parameters of the stacks required to obtain the spin accumulation from the NEGF formalism. $U_\uparrow$ and $U_\downarrow$ are the potential energies for spin-up and spin-down electrons in the ferromagnetic materials, respectively. L_{RL}, L_{B}, and L_{FL} are the thickness of the reference layer, the insulating barrier region, and the free layer, respectively. Within the barrier region, the potential energy is U_{B} and the effective electron mass is m^*_{B}. Everywhere else, the effective mass is m^*_{C}. The listed parameters are required by the Eqs. (20), (21) via (22) and (23), and by (31).

ID	L_{RL} (nm)	L_{B} (nm)	L_{FL} (nm)	$U_\uparrow$ (eV)	$U_\downarrow$ (eV)	U_{B} (eV)	m^*_{B}/m_e	m^*_{C}/m_e
A	1.1	0.7	0.9	−2.2	−0.1	1.5	0.4	0.8
B	1.1	0.8	1.2	−2.5	−0.2	1.0	0.6	0.9

is the hopping energy. The onsite energy

$$h_m(k_\perp) = \left(U_m + 2t_m + \frac{\hbar^2 k_\perp^2}{2m^*_m}\right) I_2 - \frac{J_m}{2}\boldsymbol{m}_m \cdot \boldsymbol{\sigma} \tag{21}$$

accounts for the mean potential U_m and the splitting of the potential energy J_m along the direction of the mean local magnetization $\boldsymbol{m}_m$ as well as momentum components $k_\perp$ that are perpendicular to the net current direction, i.e., the $\hat{z}$ direction and thus parallel to the interfaces. The term is constructed utilizing the Pauli matrix vector $\boldsymbol{\sigma} = (\sigma_x, \sigma_y, \sigma_z)^{\mathrm{T}}$. Within the ferromagnetic domains, the relations of the spin-up and spin-down potentials $U_\uparrow$ and $U_\downarrow$ with the mean and spin-split potentials are given by

$$U_{\mathrm{FM}} = (U_\downarrow + U_\uparrow)/2, \tag{22}$$

$$J_{\mathrm{sd}} = U_\downarrow - U_\uparrow. \tag{23}$$

The bias voltage V_b applied to the stack is assumed to vary only within the barrier domain, assumed to extend from $z = 0$ to $z = L_B$, with L_B being the thickness of the insulating layer. Therefore it changes the potential landscape of the stack according to

$$v_i = \begin{cases} -eV_b/2 & z_i \leqslant 0 \\ eV_b\, z_i/L_B - eV_b/2 & 0 < z_i < L_B \\ eV_b/2 & L_B \leqslant z_i \end{cases}. \tag{24}$$

The bias voltage is related to the shift in the chemical potentials by

$$eV_b = \mu_R - \mu_L \tag{25}$$

and is thus the shift between the occupation functions

$$f_{\mathrm{m}}(\epsilon) = \frac{1}{\exp\{\beta(\epsilon - \mu_{\mathrm{m}})\} + 1} \tag{26}$$

in the left and right leads.

1. The nonequilibrium Green's function formalism

We will now see how the spin accumulation can be calculated using the nonequilibrium Green's function formalism (NEGF), based on the work presented in Refs. [13,21,23,29]. Assuming open-boundary conditions, the retarded Green's function is

$$G^R(\epsilon, k_\perp) = [\epsilon I_{2N} - H(k_\perp) - \Sigma^R(\epsilon, k_\perp)]^{-1}. \tag{27}$$

The self-energy Σ^R function is

$$\Sigma^R_{ij}(\epsilon, k_\perp) = \begin{cases} -t_c \exp{(ik_{L,\parallel}a)} I_2 & (i = j = 0) \\ -t_c \exp{(ik_{R,\parallel}a)} I_2 & (i = j = N-1) \\ 0_{2,2} & \text{else} \end{cases} \tag{28}$$

in the case of nonmagnetic leads, or in the case of semi-infinite FM leads, the slightly more complicated spin-dependent version

$$\Sigma^R_{ij}(\epsilon, k_\perp) = \begin{cases} \Sigma^R_{\mathrm{RL}}(\epsilon, k_\perp) & (i = j = 0) \\ \Sigma^R_{\mathrm{FL}}(\epsilon, k_\perp) & (i = j = N-1) \\ 0_{2,2} & \text{else} \end{cases}, \tag{29}$$

with

$$\Sigma^R_m(\epsilon, k_\perp) = -t_m R(\boldsymbol{m}_m) \begin{bmatrix} \exp{(ik^\uparrow_m a)} & 0 \\ 0 & \exp{(ik^\downarrow_m a)} \end{bmatrix} R(\boldsymbol{m}_m)^\dagger. \tag{30}$$

Here $R(\hat{n})$ is the rotation matrix from the z direction to $\hat{n}$. The wave number parallel to the net-transport direction is given by

$$k^\sigma_{m,\parallel} = \sqrt{\frac{2m^*_m}{\hbar^2}\left(\epsilon - U^\sigma_m\right) - k^2_\perp}. \tag{31}$$

The in-scattering function (33) or (32) is obtained from anti-Hermitian part of (28) or (29), respectively, and is weighted by the occupation functions of the left and right lead, which are just the Fermi-Dirac distribution shifted by $\mp V_b/2$:

$$\Sigma^{\mathrm{in}}_{ij}(\epsilon, k_\perp) = \begin{cases} f_L(\epsilon) 2t_c \sin(k_{L,\parallel}a) I_2 & i = j = 0 \\ f_R(\epsilon) 2t_c \sin(k_{R,\parallel}a) I_2 & j = i = N-1 \\ 0_{2,2} & \text{else} \end{cases} \tag{32}$$

in the case of nonmagnetic leads or

$$\Sigma^{\mathrm{in}}_{ij}(\epsilon, \epsilon_\parallel) = \begin{cases} i f_{\mathrm{RL}}(\epsilon)\left(\Sigma^R_{\mathrm{RL}}(\epsilon_\parallel) - \Sigma^{R\dagger}_{\mathrm{RL}}(\epsilon_\parallel)\right) & i = j = 0 \\ i f_{\mathrm{FL}}(\epsilon)\left(\Sigma^R_{\mathrm{FL}}(\epsilon_\parallel) - \Sigma^{R\dagger}_{\mathrm{FL}}(\epsilon_\parallel)\right) & j = i = N-1 \\ 0_{2,2} & \text{else} \end{cases} \tag{33}$$

in the case of ferromagnetic leads. The full nonequilibrium Green's function is

$$G^n(\epsilon) = D_{\mathrm{2D}}(\epsilon) \int G^R(\epsilon, k_\perp) \Sigma^{in}(\epsilon, k_\perp) G^{R\dagger}(\epsilon, k_\perp) dk_\perp, \tag{34}$$

with $D_{2D}(\epsilon)$ being the two-dimensional density of states. The diagonal elements of Eq. (34) are the local densities such that

$$s_k(z_i) = -\frac{\mu_B}{2\pi a} \int \mathrm{Tr}_\sigma \left[G^n_{ii}(\epsilon)\sigma_k\right] d\epsilon \tag{35}$$

yields the spin accumulation [23,24].

2. Equivalence to solutions obtained from the Schrödinger equation

The nonequilibrium Green's function is a sort of correlation function with its entries being [29]

$$G^{n\,\sigma\sigma'}_{ij} = 2\pi a \sum_{\sigma''} \sum_k \psi_k^{\sigma(\sigma'')}(z_i)\overline{\psi_k^{\sigma(\sigma'')}(z_j)}, \tag{36}$$

where the sums are over electrons k entering the problem region from the left and the right lead and both incident spin states. Here we adopted the notation from [30] and indicate the incident spin state in parentheses. For the case of completely coherent transport, it is relatively straightforward to show the equivalence of solving (27) and then evaluating (34) to solving the time-independent Schrödinger equation,

$$[\epsilon - \hat{H}(z)]|\psi_k^{(\sigma)}(z)\rangle = 0 \tag{37}$$

with

$$\left|\psi_k^{(\sigma)}(z)\right\rangle = \begin{bmatrix} \psi_k^{\uparrow(\sigma)}(z) \\ \psi_k^{\downarrow(\sigma)}(z) \end{bmatrix} \tag{38}$$

numerically or analytically [24], and doing so is very instructive to understand the formalism used.

Let us focus on an electron entering from the left nonmagnetic lead in the spin-up state. If one was going to solve the Schrödinger equation analytically, the ansatz in the left lead would be

$$\psi_{\mathrm{L}}^{\uparrow(\uparrow)}(z)|_{z\in\Omega_{\mathrm{L}}} = A_{\mathrm{L}}[e^{ik_{\mathrm{L}}^{\uparrow}x} + r^{\uparrow}e^{-k_{\mathrm{L}}^{\uparrow}x}], \tag{39}$$

$$\psi_{\mathrm{L}}^{\downarrow(\uparrow)}(z)|_{z\in\Omega_{\mathrm{L}}} = r^{\downarrow}e^{-k_{\mathrm{L}}^{\downarrow}x}, \tag{40}$$

and

$$\psi_{\mathrm{L}}^{\uparrow(\uparrow)}(z)|_{z\in\Omega_{\mathrm{R}}} = u^{\uparrow}e^{ik_{\mathrm{R}}^{\uparrow}x}, \tag{41}$$

$$\psi_{\mathrm{L}}^{\downarrow(\uparrow)}(z)|_{z\in\Omega_{\mathrm{R}}} = u^{\downarrow}e^{ik_{\mathrm{R}}^{\downarrow}x}, \tag{42}$$

in the right lead. We are now going to determine the open-boundary conditions. In an effort to keep the notation in the following argumentation clean, the indices specifying the incident lead and wave number are dropped.

For electrons entering from the left, only an outgoing wave has to be accounted for on the right boundary. Since the boundary conditions should allow for an unobstructed propagation outwards of the problem region into a homogeneous semi-infinite lead, the equation at the boundary node $N-1$,

$$t_{\mathrm{R}}|\psi_{N-2}\rangle + (\epsilon I_2 - h_{\mathrm{R}})|\psi_{N-1}\rangle + t_{\mathrm{R}}|\psi_N\rangle = 0, \tag{43}$$

can be simplified with

$$|\psi_N\rangle = e^{ik_{\mathrm{R}}a}|\psi_{N-1}\rangle \tag{44}$$

to

$$t_{\mathrm{R}}|\psi_{N-2}\rangle + [(\epsilon + t_{\mathrm{R}}e^{ik_{\mathrm{R}}a})I_2 - h_{\mathrm{R}}]|\psi_{N-1}\rangle = 0. \tag{45}$$

Equation (44) is justified since in the region of the right lead, the wave function is of the form (41).

The situation at the left boundary involves not only an outgoing reflected part of the wave function but also the incident wave in the spin-up component, and we therefore not only need the equation centered on node 0,

$$t_{\mathrm{L}}|\psi_{-2}\rangle + (\epsilon I_2 - h_{\mathrm{L}})|\psi_{-1}\rangle + t_{\mathrm{L}}|\psi_0\rangle = 0, \tag{46}$$

but also on node -1,

$$t_{\mathrm{L}}|\psi_{-1}\rangle + (\epsilon I_2 - h_{\mathrm{L}})|\psi_0\rangle + t_{\mathrm{L}}|\psi_1\rangle = 0, \tag{47}$$

to eliminate the additional unknown. To do so one requires the tight-binding relation

$$(\epsilon - h) = -t(e^{ika} + e^{-ika}). \tag{48}$$

After some calculations presented in the Appendix, one obtains

$$t_{\mathrm{L}}A_{\mathrm{L}}(1 - e^{i2k_{\mathrm{L}}a}) + t_{\mathrm{L}}\psi_0^{\uparrow}e^{ik_{\mathrm{L}}a} + (\epsilon - h_{\mathrm{L}})\psi_0^{\uparrow} + t_{\mathrm{L}}\psi_1^{\uparrow} = 0 \tag{49}$$

for the spin-up component at the left boundary. This equation contains a term equivalent to the one obtained for the right boundary, but also an additional source term

$$S = -t_{\mathrm{L}}A_{\mathrm{L}}(1 - e^{i2k_{\mathrm{L}}a}). \tag{50}$$

The spin-down component can be treated like the spin-up component at the right boundary, and thus the equation for the left boundary can be written as

$$[(\epsilon + t_{\mathrm{L}}e^{ik_{\mathrm{L}}a})I_2 - h_{\mathrm{L}}]|\psi_0\rangle + t_{\mathrm{L}}|\psi_1\rangle = \begin{bmatrix} S \\ 0 \end{bmatrix}, \tag{51}$$

and the full problem for electrons entering from the left in the spin-up state is therefore stated by the system of equations (52):

$$\begin{aligned} &[(\epsilon + t_{\mathrm{L}}e^{ik_{\mathrm{L}}a})I_2 - H_{00}]|\psi_0\rangle - H_{01}|\psi_1\rangle = \begin{bmatrix} S \\ 0 \end{bmatrix} \\ &-H_{i\,i-1}|\psi_{i-1}\rangle + (\epsilon I_2 - H_{ii})|\psi_i\rangle - H_{i\,i+1}|\psi_{i+1}\rangle = 0,\ 1 \leqslant i \leqslant N-2 \\ &-H_{N-1\,N-2}|\psi_{N-2}\rangle + [(\epsilon + t_{\mathrm{R}}e^{ik_{\mathrm{R}}a})I_2 - H_{N-1\,N-1}]|\psi_{N-1}\rangle = 0. \end{aligned} \tag{52}$$

The solution of this tridiagonal system together with the one for electrons entering from the right and for both incident spin states yields the same spin accumulation as the one obtained from the nonequilibrium Green's function formalism. This

equivalence of the two approaches can be shown by starting from the integrand of (34):

$$G^n_{ij} = \sum_{k=0}^{N-1}\sum_{l=0}^{N-1} G^R_{ik}\Sigma^{\text{in}}_{kl}G^A_{lj} \tag{53}$$

$$= \sum_{k=0}^{N-1} G^R_{ik}\left[\Sigma_L\delta_{k0}G^A_{0j} + \Sigma_R\delta_{k\,N-1}G^A_{N-1\,j}\right] \tag{54}$$

$$= G^R_{i0}\Sigma_L G^A_{0j} + G^R_{i\,N-1}\Sigma_R G^A_{N-1\,j} \tag{55}$$

$$= G^R_{i0}\Sigma_L\overline{G^R}_{j0} + G^R_{i\,N-1}\Sigma_R\overline{G^R}_{j\,N-1}. \tag{56}$$

The first part is the contribution of electrons entering from the left. Here, the only relevant part of G^R is its first column, which is the solution to a subproblem of (27):

$$\sum_{j=0}^{N-1}\left[\epsilon\delta_{ij} - H_{ij} - \Sigma^R_{ij}\right]G^R_{j0} = \delta_{i0}I_2. \tag{57}$$

This can be compared to the system of equations (52), which can be rewritten as

$$\sum_{j=0}^{N-1}\left[\epsilon\delta_{ij} - H_{ij} - \Sigma^R_{ij}\right]|\psi^{(\uparrow)}_j\rangle = \begin{bmatrix} S \\ 0 \end{bmatrix}\delta_{i0}, \tag{58}$$

and the first column of the retarded Green's function is related to the wave function of an electron entering from the left by

$$G^R_{j0}\,S = [|\psi^{(\uparrow)}_j\rangle, |\psi^{(\downarrow)}_j\rangle], \tag{59}$$

which is not surprising, since $S\delta_{i0}$ could be viewed as a source term and convolution with the problem's Green's function should therefore yield the full solution of the problem.

Judging from (36), (56), and (59), the in-scattering matrix is proportional to the square norm of the source term (50), which in turn is proportional to the square norm of the incoming wave function's amplitude $|A_\text{L}|^2$. Plugging in the one-dimensional density of states times the occupation function for $|A_\text{L}|^2$ and knowing that the derivative of (48) is

$$\hbar v = 2at\,\sin(ka) \tag{60}$$

yields the square norm of the source term,

$$|S|^2 = t_\text{L}^2|A_\text{L}|^2(1 - e^{i2ka})(1 - e^{-i2ka}) \tag{61}$$

$$= t_\text{L}^2 f(\epsilon)\frac{m^*}{2\pi\hbar^2 k}(1 - e^{i2ka})(1 - e^{-i2ka}) \tag{62}$$

$$= t_\text{L}^2 f(\epsilon)\frac{1}{2\pi\hbar v}4\sin^2(ka) \tag{63}$$

$$= \frac{1}{2\pi a}2t_\text{L}f(\epsilon)\sin(ka), \tag{64}$$

and shows the equivalence of the solution of the tridiagonal system and the nonequilibrium Green's function formalism as well as the validity of (36). This argumentation can also be adopted for magnetic leads by having a spin-dependent wave number and density of states and rotating the self-energy matrices Σ^R and the source term according to the local magnetization direction [31].

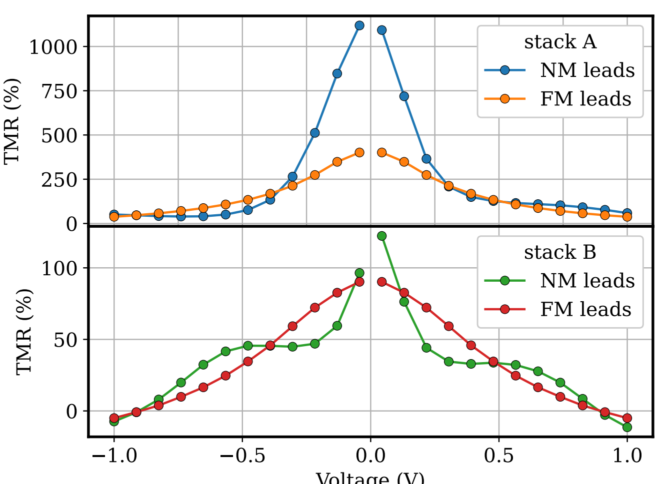

FIG. 2. The voltage dependence of the TMR effect for both stacks, considering the effects of the NM/FM interfaces (NM leads) and omitting them (FM leads). The curves were obtained solely from the free-electron model for fixed parallel and antiparallel configurations of $\boldsymbol{m}_\text{RL}$ and $\boldsymbol{m}_\text{FL}$.

III. RESULTS

We will now compare the transport properties of the two stacks A and B. Figure 2 shows the voltage dependence of the TMR of stack A and B obtained from the NEGF using a Hamiltonian with five domains with NM leads and a three-domain Hamiltonian with semi-infinite FM leads.

Similarly, the voltage dependence for the averaged fieldlike and dampinglike torque acting on the free layer of both stacks is shown in Fig. 3 for both types of Hamiltonian. The field components were calculated for $\boldsymbol{m}_\text{RL} \parallel \hat{x}$ and $\boldsymbol{m}_\text{FL} \parallel \hat{z}$. Since that means that $\theta = \angle\boldsymbol{m}_\text{RL}, \boldsymbol{m}_\text{FL} = \pi/2$, the torque components are related to the field components by $\tau_\text{dl} = -\gamma H_\text{dl}(\theta = \pi/2)$ and $\tau_\text{fl} = -\gamma H_\text{fl}(\theta = \pi/2)$. While the field components H_fl and H_dl depend on the angle θ between $\boldsymbol{m}_\text{RL}$ and $\boldsymbol{m}_\text{FL}$, the torque components τ_fl and τ_dl are constants for a fixed

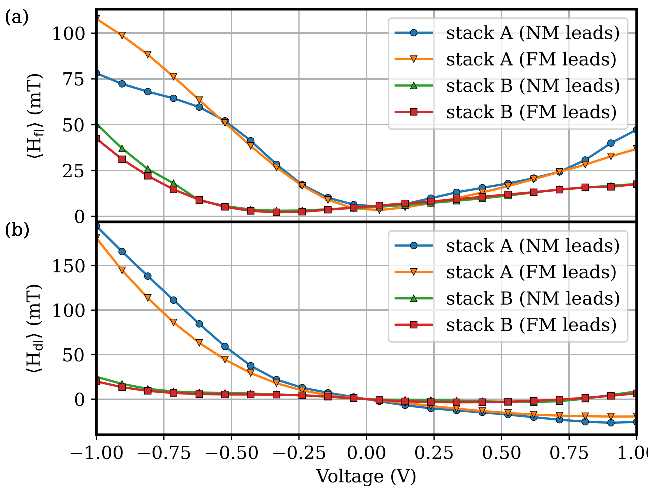

FIG. 3. Average values of H_fl and H_dl acting on the magnetization of the free layer for $\boldsymbol{m}_\text{RL} \perp \boldsymbol{m}_\text{FL}$. For stack B the dampinglike component has an additional sign reversal around 0.75 V.

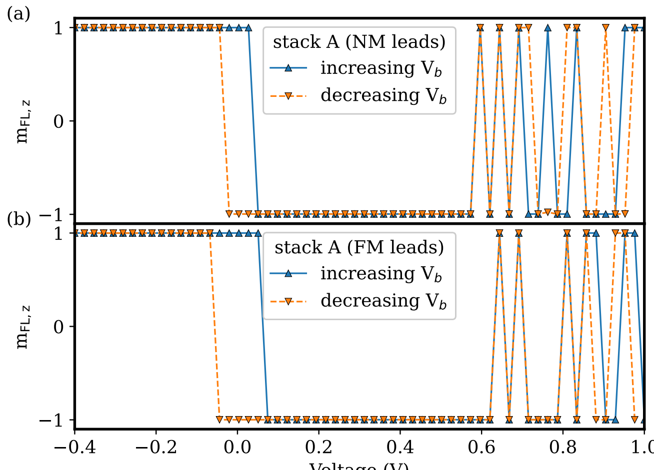

FIG. 4. Simulation of the STT-induced switching behavior of stack A for (a) a five-domain Hamiltonian with NM leads and (b) a three-domain Hamiltonian with FM leads. The hysteresis includes back-hopping that appears as a dynamic effect. The free-layer out-of-plane component was sampled after first applying the indicated voltage for 60 ns and then letting the system relax for 30 ns. After the reference layer is fully relaxed, $m_z = 1$ corresponds to the low-resistance state and $m_z = -1$ to the high-resistance state.

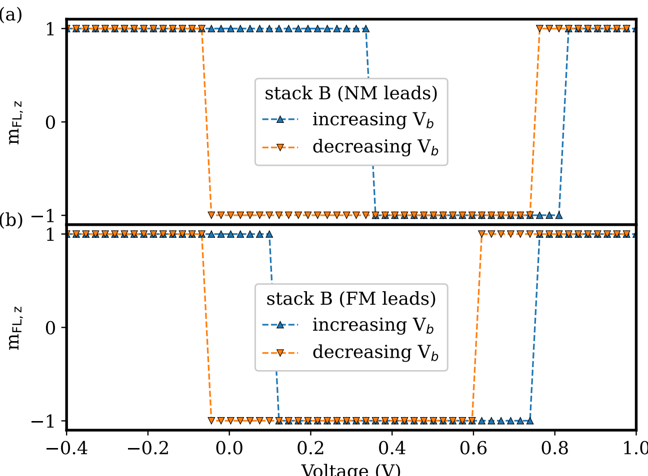

FIG. 5. Simulation of the STT-induced switching behavior of stack B for (a) a five-domain Hamiltonian with NM leads and (b) a three-domain Hamiltonian with FM leads. Due to the additional change of sign of the dampinglike torque component, the hysteresis includes a second loop on the positive-voltage branch. The data was obtained in the same manner as in the data depicted in Fig. 4.

value of the bias voltage. Figure 3 shows a trend reversal of the dampinglike component for stack B that results in an additional change of sign around 0.8 V in the case of the five-domain Hamiltonian and around 0.75 V in the case of the three-domain Hamiltonian. It is noteworthy that while the inclusion of reflexions from the FM/NM interfaces results in vastly different TMR curves with an unexpected nonmonotonic behavior for stack B, the number of domains included into the device Hamiltonian does not result in a qualitative change in the torque component voltage dependence.

However, the additional change of sign of the dampinglike torque for stack B leads to very different switching behavior compared to the one observed for stack A. This can be seen by comparing the respective M-V hysteresis curves of stacks A and B in Figs. 4 and 5, respectively.

The data shown in Figs. 4 and 5 was obtained in the following way: First a bias voltage V_b was applied for 60 ns. During this time, the STT acts on both the reference and the free layer of the stack. Next the voltage was cut off and the system was allowed to relax for a time frame of 30 ns, after which $\boldsymbol{m}_{\mathrm{FL}}$ was sampled. These data points are indicated by markers. The procedure was then repeated with the next voltage value, starting from the lowest voltage $V_{b,\mathrm{min}}$ and increasing it from step to step up to a maximum value $V_{b,\mathrm{max}}$. Then, after reaching this maximum value, the voltage was decreased in the same manner back to the starting value $V_{b,\mathrm{min}}$.

Values of the free-layer out-of-plane component equal to 1 correspond to the low-resistance state, while values equal to −1 correspond to the high-resistance state. After the system is fully relaxed, these states are indeed well defined, since the exchange coupling acting on the reference layer will always let its magnetization relax into the positive z direction.

The hysteresis of stack A depicted in Fig. 4 features what is usually referred to as back-hopping on the positive-voltage branch (P → AP switching). For voltages $V_b \geqslant 0.6$ V, the sampled free-layer magnetization starts switching between the parallel and antiparallel state in a seemingly random fashion, reminiscent of the back-hopping measured in [10]. As we will see later, the back-hopping in our simulations is due to the reference layer itself changing direction when subjected to large enough torques in a dynamic process outlined with similar numerical methods in [16,17].

Comparison with Fig. 5 reveals that stack B behaves very differently. The additional change in sign of the dampinglike torque component gives rise to a complete second hysteresis loop, as we have already argued in a previous work [25] and akin to measurements shown in Ref. [19]. This apparent similarity does not necessarily indicate that the second loop seen in Ref. [19] arises from a quadratic dampinglike term, however. In their time-resolved measurements, Devolder *et al.* found the MRAM cell to first switch as intended from the P to the AP state, but then in a second switching event it switches back into a low-resistance state. They found this state to relax back into the AP state as soon as the bias voltage was removed. The magnetization reversal seen in Fig. 5 is, however, stable and is not entered by a P → AP → P transition at a single voltage but in a hysteretic manner. From their analysis, Devolder *et al.* concluded that the back-hopping observed by them is due to the destabilization of the reference system, although the expected back-and-forth switching did not occur.

We are now focusing on the dynamic effect leading to the back-hopping in Fig. 4. For positive voltages, the STT aims to have the free-layer magnetization aligned antiparallel with the magnetization of the reference layer. However, the torque acting on the reference layer tries to align its magnetization parallel with the free-layer magnetization. While the system is in its parallel state, this means that the reference layer is indeed stabilized by the STT, but as soon as the free layer is switched to its antiparallel configuration, the contrary is the case. Preferably for most applications, anisotropy and

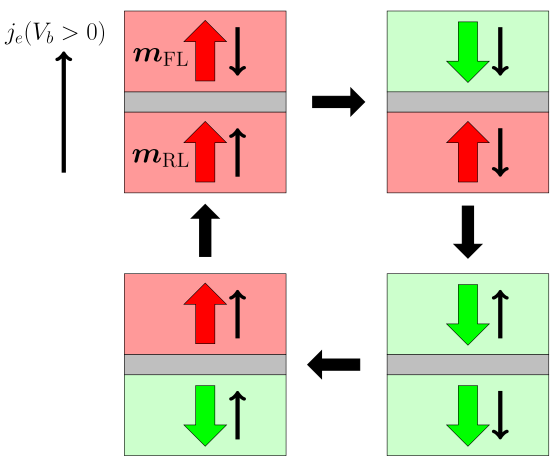

FIG. 6. Cyclic process of back-hopping due to switching of the reference layer. Large arrows indicate the magnetization of the layers, while the small arrows indicate the energetically preferred direction due to STT.

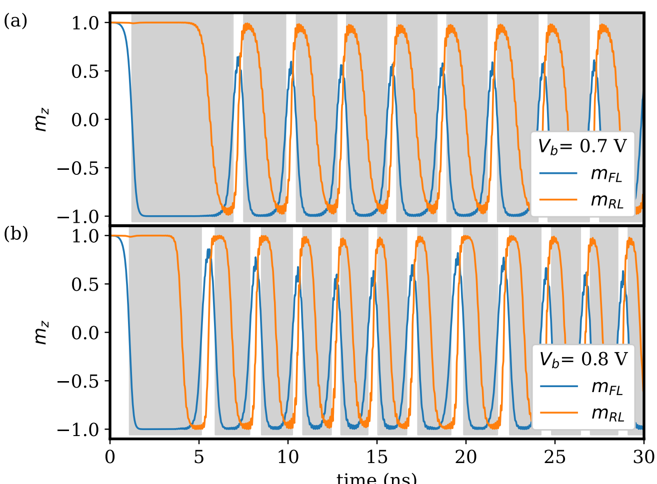

FIG. 7. Dynamics of the out-of-plane component of free and reference layer for stack A at $V_b = 0.7$ V and $V_b = 0.8$ V. Gray regions mark time intervals in which cutting of the voltage spontaneously would lead to successful P $\rightarrow$ AP switching if the two magnetizations were uncoupled. This is because the reference-layer magnetization always relaxes back into the positive out-of-plane direction, i.e., the positive z direction, due to the interlayer-exchange coupling to the remaining reference system. Consequently, a free-layer magnetization that relaxed into the positive z direction would therefore result in the low-resistance P state, while a free-layer magnetization that has relaxed into the negative z direction would result in the high-resistance state.

interlayer exchange would keep the reference system stable, but the torque acting on the reference layer in stack A at large voltages outweighs these stabilizing field contributions. The consequence is what can be thought of as a cyclic process [18] as depicted in Fig. 6. First, the system is in its parallel configuration and the reference layer is stabilized along the positive z direction. The free layer is then switched from parallel to antiparallel by the STT, destabilizing the reference layer. In turn, the reference layer switches to the negative z direction so that its magnetization is parallel to the free-layer magnetization again, mirroring the original state.

Figure 7 shows the dynamics of the out-of-plane magnetization components for both layers in stack A at 0.7 and 0.8 V, and can be easily compared to the process illustrated in Fig. 6. Additionally, a three-dimensional animation that shows the first full cycle of the back-hopping seen in Fig. 7(b) can be found in the Supplemental Material [32]. Since the dampinglike torque for stack A is a monotone function of the bias voltage within the considered voltage interval, the precessional switching dynamics of both $\boldsymbol{m}_{\rm FL}$ and $\boldsymbol{m}_{\rm RL}$ become faster when the voltage is increased. Similarly, Fig. 8 shows the effect of the Gilbert damping parameter α on the back-hopping. Figure 8 indicates that a smaller value of the damping parameter allows for a faster switching dynamics and reduces the voltage limit for the back-hopping effect to occur.

The gray areas in Figs. 7 and 8 indicate time intervals in which cutting off the voltage would result in "correct" switching, i.e., a free-layer magnetization that relaxes into the negative z direction, if $\boldsymbol{m}_{\rm RL}$ and $\boldsymbol{m}_{\rm FL}$ would be uncoupled when no voltage is applied. However, the fieldlike torque in Fig. 3 does not vanish at zero bias voltage and therefore acts effectively as a form of interlayer coupling.

In contrast to the free layer, the reference layer always relaxes in the positive z direction, since the bias interlayer exchange coupling is the dominant field contribution over the anisotropy field and the interlayer coupling exerted by the fieldlike torque term. Thus a measurement would indeed always yield the low-resistance (P) state when the free layer relaxed into the positive z direction and the high-resistance (AP) state when the free layer relaxed into the negative z direction.

Since the final state of the free layer is thus determined by the time the voltage is applied, it might appear to be somewhat random. Assuming that the actual time the voltage is applied is distributed around a mean value μ, one can calculate the

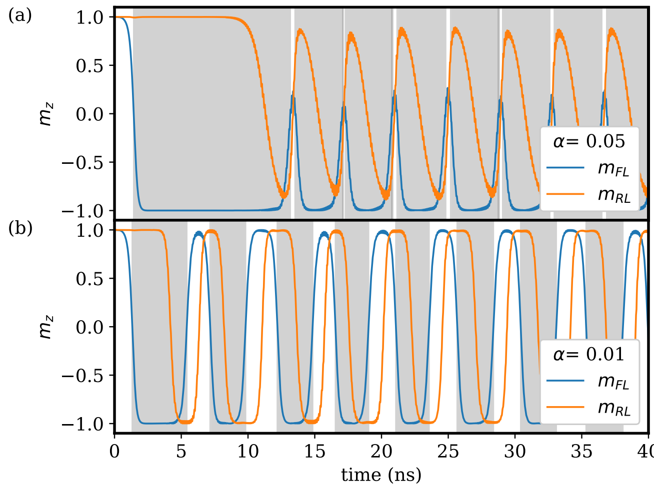

FIG. 8. Dynamics of the out-of-plane magnetization component of the free and reference layer for stack A at $V_b = 0.6$ V for two different values of the damping parameter. (a) For $\alpha = 0.05$, which is the value used to obtain the hysteresis curves in this work, the back-hopping effect starts to occur slightly below $V_b = 0.6$ V. (b) A smaller damping parameter reduces the voltage limit for the back-hopping.

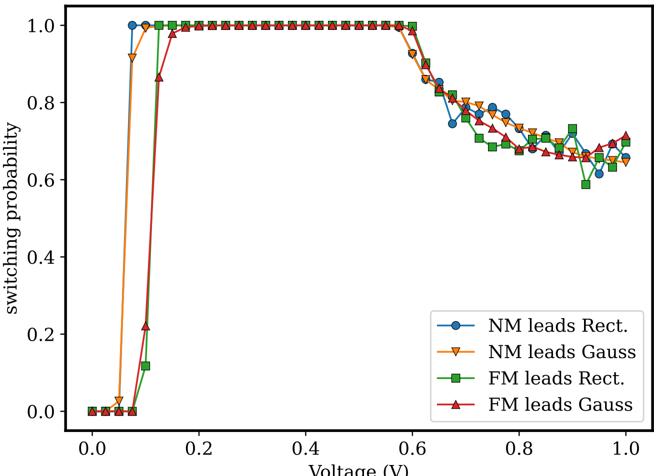

FIG. 9. Approximated P → AP switching probability for stack A, assuming the switching pulse duration is distributed according to a rectangular distribution with $\mu = 18$ ns and $L = 4$ ns (blue circles for NM leads, green squares for FM leads) and a Gaussian distribution with $\mu = 18$ ns and $\sigma = 4$ ns (orange downward triangles for NM leads and red upward triangles for FM leads).

switching probability by convolution of the signal

$$s(t) = \begin{cases} 1 & m_{z,\mathrm{FL}}(t) > 0 \\ 0 & \text{else} \end{cases} \tag{65}$$

with the distribution function. Note that the background coloring of Fig. 7 does conform to the signal function (65). The approximated P → AP switching probability of stack A obtained for a Gaussian distribution as well as for a rectangular distribution can be found in Fig. 9. It shows a sudden reduction of the success rate for voltages above 0.55 V with a further decrease for higher values of V_b as a result of the quicker oscillation of $\boldsymbol{m}_{\mathrm{RL}}$ and $\boldsymbol{m}_{\mathrm{FL}}$. The exact form of the pronounced nonmonotonic behavior seen in Fig. 9 depends strongly on the mean value and is due to the similar length of the distribution and the binary pulses of the signal (65).

IV. CONCLUSION

In this work we investigated two possible origins of the back-hopping effect—the first being the destabilization and possible switching of the reference layer due to the STT acting on it, and the second one being an additional sign reversal of the dampinglike torque term for large voltages due to its quadratic nature. Both were modeled and investigated with stack A showing the dynamic effect of cyclic reference and free-layer switching, while the second sign reversal of the dampinglike torque for stack B leads to a second hysteresis loop. This implies that in experiments where the back-hopping appears as chaotic back-and-forth switching between the high- and low-resistance state, it cannot be attributed to an additional change of sign of the dampinglike torque, as this characteristic would yield a complete second hysteresis loop instead.

If the back-hopping is then because of the dynamic process described here or in Refs. [16–18], one should note that in the case of separated pulses for reading and writing, the reference layer would rotate back into the direction favored by the interlayer exchange coupling (assuming that it is large enough to overcome the effective anisotropy) after the writing pulse ended. This means that the high- and low-resistance states would still correspond to well-defined configurations. Meanwhile, measuring the resistance for the writing current would lead to data with a more ambiguous state of the reference layer. Still, one should remember that the P and AP resistances could differ depending on the direction of the reference layer relative to the magnetization of the remaining hard layer stack [19].

ACKNOWLEDGMENTS

The authors extend their gratitude to Aurélien Manchon for the valuable insight he provided. This research was enabled by the financial support of the Austrian Science Fund (FWF) I 4917-N and I 6068-N.

APPENDIX

Our aim is to show how the tridiagonal system (52) for electrons entering from the left lead in the spin-up state is obtained in detail. Specifically, this means to determine the concrete form of the open-boundary conditions.

If the problem region was not restricted to a region close to the actual device, the discrete form of the Schrödinger equation would read

$$t_m|\psi_{n-1}\rangle + (\epsilon I_2 - h_m)|\psi_n\rangle + t_m|\psi_{n+1}\rangle = 0, \quad m \in \{\mathrm{L}, \mathrm{R}\} \tag{A1}$$

for every node n located within the homogeneous semi-infinite nonmagnetic wires. Within these wires, Eqs. (39)–(42) are the components of solutions to the Schrödinger equation. We are not going to reiterate how the right boundary condition is calculated, since this is fully covered in the main text. However, for the spin-up component at the left boundary, we have to eliminate the coefficient of the reflected part r, which we will detail now.

By plugging the ansatz (39) into the equation for node $n = -1$ we can calculate the reflected amplitude:

$$t_\mathrm{L}\psi_{-2}^\uparrow + (\epsilon - h_\mathrm{L})\psi_{-1}^\uparrow + t_\mathrm{L}\psi_0^\uparrow = 0, \tag{A2}$$

$$t_\mathrm{L}A_\mathrm{L}[e^{-ik_\mathrm{L}a} + re^{ik_\mathrm{L}a}] + (\epsilon - h_\mathrm{L})A_\mathrm{L}[1 + r] + t_\mathrm{L}\psi_0^\uparrow = 0, \tag{A3}$$

$$t_\mathrm{L}A_\mathrm{L}e^{-ik_\mathrm{L}a} + rA_\mathrm{L}[t_\mathrm{L}e^{ik_\mathrm{L}a} + (\epsilon - h_\mathrm{L})] + (\epsilon - h_\mathrm{L})A_\mathrm{L} + t_\mathrm{L}\psi_0^\uparrow = 0, \tag{A4}$$

$$rA_\mathrm{L}[t_\mathrm{L}e^{ik_\mathrm{L}a} + (\epsilon - h_\mathrm{L})] = -t_\mathrm{L}A_\mathrm{L}e^{-ik_\mathrm{L}a} - (\epsilon - h_\mathrm{L})A_\mathrm{L} - t_\mathrm{L}\psi_0^\uparrow, \tag{A5}$$

$$rA_\mathrm{L} = \frac{-t_\mathrm{L}A_\mathrm{L}e^{-ik_\mathrm{L}a} - (\epsilon - h_\mathrm{L})A_\mathrm{L} - t_\mathrm{L}\psi_0^\uparrow}{t_\mathrm{L}e^{ik_\mathrm{L}a} + (\epsilon - h_\mathrm{L})}. \tag{A6}$$

This reflected amplitude can be rewritten as

$$rA = -A_{\mathrm{L}} e^{i2k_{\mathrm{L}}a} + \psi_0 \, e^{ik_{\mathrm{L}}a}, \tag{A7}$$

utilizing the tight-binding dispersion (48). We look now at the next equation, centered on the left boundary node $n = 0$, and plug in the above coefficient:

$$t_{\mathrm{L}}\psi_{-1}^{\uparrow} + (\epsilon - h_{\mathrm{L}})\psi_0^{\uparrow} + t_{\mathrm{L}}\psi_1^{\uparrow} = 0, \tag{A8}$$

$$t_{\mathrm{L}}A_{\mathrm{L}}[1 + r] + (\epsilon - h_{\mathrm{L}})\psi_0^{\uparrow} + t_{\mathrm{L}}\psi_1^{\uparrow} = 0, \tag{A9}$$

$$t_{\mathrm{L}}[A_{\mathrm{L}} - A_{\mathrm{L}}e^{i2k_{\mathrm{L}}a} + \psi_0^{\uparrow}\, e^{ik_{\mathrm{L}}a}] + (\epsilon - h_{\mathrm{L}})\psi_0^{\uparrow} + t_{\mathrm{L}}\psi_1^{\uparrow} = 0, \tag{A10}$$

$$t_{\mathrm{L}}A_{\mathrm{L}}(1 - e^{i2k_{\mathrm{L}}a}) + t_{\mathrm{L}}\psi_0^{\uparrow}e^{ik_{\mathrm{L}}a} + (\epsilon - h_{\mathrm{L}})\psi_0^{\uparrow} + t_{\mathrm{L}}\psi_1^{\uparrow} = 0. \tag{A11}$$

By identifying $-t_{\mathrm{L}}A_{\mathrm{L}}(1 - e^{i2k_{\mathrm{L}}a})$ as a source term, we obtain the set of equations (52) for electrons entering from the left. The same can be done for electrons entering the problem region from the right lead.

[1] T. McKinnon, B. Heinrich, and E. Girt, J. Magn. Magn. Mater. **546**, 168646 (2022).
[2] M. Julliere, Phys. Lett. A **54**, 225 (1975).
[3] T. Miyazaki and N. Tezuka, J. Magn. Magn. Mater. **139**, L231 (1995).
[4] Y. Huai, AAPPS Bull. **18**, 33 (2008).
[5] S. Bhatti, R. Sbiaa, A. Hirohata, H. Ohno, S. Fukami, and S. Piramanayagam, Mater. Today **20**, 530 (2017).
[6] Y. Huai, F. Albert, P. Nguyen, M. Pakala, and T. Valet, Appl. Phys. Lett. **84**, 3118 (2004).
[7] J. C. Slonczewski, Phys. Rev. B **39**, 6995 (1989).
[8] L. Berger, Phys. Rev. B **54**, 9353 (1996).
[9] J. Slonczewski and J. Sun, J. Magn. Magn. Mater. **310**, 169 (2007).
[10] T. Min, J. Z. Sun, R. Beach, D. Tang, and P. Wang, J. Appl. Phys. **105**, 07D126 (2009).
[11] S.-C. Oh, S.-Y. Park, A. Manchon, M. Chshiev, J. Han, H.-W. Lee, J.-E. Lee, K.-T. Nam, Y. Jo, Y.-C. Kong, B. Dieny, and K.-J. Lee, Nat. Phys. **5**, 898 (2009).
[12] J. Sun, M. Gaidis, G. Hu, E. O'Sullivan, S. Brown, J. Nowak, P. Trouilloud, and D. Worledge, J. Appl. Phys. **105**, 07D109 (2009).
[13] I. Theodonis, N. Kioussis, A. Kalitsov, M. Chshiev, and W. H. Butler, Phys. Rev. Lett. **97**, 237205 (2006).
[14] A. Kalitsov, M. Chshiev, I. Theodonis, N. Kioussis, and W. H. Butler, Phys. Rev. B **79**, 174416 (2009).
[15] H. Kubota, A. Fukushima, K. Yakushiji, T. Nagahama, S. Yuasa, K. Ando, H. Maehara, Y. Nagamine, K. Tsunekawa, D. D. Djayaprawira, N. Watanabe, and Y. Suzuki, Nat. Phys. **4**, 37 (2008).
[16] Z. Hou, Y. Liu, S. Cardoso, P. P. Freitas, H. Chen, and C.-R. Chang, J. Appl. Phys. **109**, 113914 (2011).
[17] C. Safranski and J. Z. Sun, Phys. Rev. B **100**, 014435 (2019).
[18] C. Abert, H. Sepehri-Amin, F. Bruckner, C. Vogler, M. Hayashi, and D. Suess, Phys. Rev. Appl. **9**, 054010 (2018).
[19] T. Devolder, O. Bultynck, P. Bouquin, V. D. Nguyen, S. Rao, D. Wan, B. Sorée, I. P. Radu, G. S. Kar, and S. Couet, Phys. Rev. B **102**, 184406 (2020).
[20] S. Datta, Superlattices Microstruct. **28**, 253 (2000).
[21] D. Datta, B. Behin-Aein, S. Salahuddin, and S. Datta, in *2010 IEEE International Electron Devices Meeting (IEDM)* (IEEE, New York, 2011), pp. 22.8.1–22.8.4.
[22] S. Salahuddin and S. Datta, Appl. Phys. Lett. **89**, 153504 (2006).
[23] A. Kalitsov, I. Theodonis, N. Kioussis, M. Chshiev, W. H. Butler, and A. Vedyayev, J. Appl. Phys. **99**, 08G501 (2006).
[24] M. Chshiev, A. Manchon, A. Kalitsov, N. Ryzhanova, A. Vedyayev, N. Strelkov, W. H. Butler, and B. Dieny, Phys. Rev. B **92**, 104422 (2015).
[25] P. Flauger, C. Abert, and D. Suess, Phys. Rev. B **105**, 134407 (2022).
[26] H. Zhao, B. Glass, P. K. Amiri, A. Lyle, Y. Zhang, Y.-J. Chen, G. Rowlands, P. Upadhyaya, Z. Zeng, J. A. Katine, J. Langer, K. Galatsis, H. Jiang, K. L. Wang, I. N. Krivorotov, and J.-P. Wang, J. Phys. D **45**, 025001 (2012).
[27] S. Yuasa and D. Djayaprawira, J. Phys. D **40**, R337 (2007).
[28] R. K. Mains, I. Mehdi, and G. I. Haddad, Appl. Phys. Lett. **55**, 2631 (1989).
[29] S. Datta, *Electronic Transport in Mesoscopic Systems*, 1st ed., Cambridge Studies in Semiconductor Physics and Microelectronic Engineering (Cambridge University Press, Cambridge, England, 1995).
[30] A. Manchon, N. Ryzhanova, A. Vedyayev, M. Chschiev, and B. Dieny, J. Phys.: Condens. Matter **20**, 145208 (2008).
[31] A. A. Yanik, G. Klimeck, and S. Datta, Phys. Rev. B **76**, 045213 (2007).
[32] See Supplemental Material at http://link.aps.org/supplemental/10.1103/PhysRevB.108.014430 for a three-dimensional animation of $\boldsymbol{m}_{\mathrm{FL}}$ and $\boldsymbol{m}_{\mathrm{RL}}$ that shows the first full cycle of the back-hopping in stack A at a bias voltage of 0.8 V.